Science of the Total Environment 648 (2019) 1639–1648

Contents lists available at ScienceDirect

Science of the Total Environment

journal homepage: www.elsevier.com/locate/scitotenv

Comparison of integrated water vapor from GNSS and radiosounding at four GRUAN stations

Javier Vaquero-Martínez[a,b,*], Manuel Antón[a,b], José Pablo Ortiz de Galisteo[c,d], Roberto Román[d], Victoria E. Cachorro[d], David Mateos[d]

[a] Departamento de Física, Universidad de Extremadura, Badajoz, Spain
[b] Instituto Universitario de Investigación del Agua, Cambio Climático y Sostenibilidad (IACYS), Universidad de Extremadura, Badajoz, Spain
[c] Agencia Estatal de Meteorología (AEMET), Valladolid, Spain
[d] Grupo de Óptica Atmosférica, Universidad de Valladolid, Valladolid, Spain

HIGHLIGHTS

- GRUAN's GNSS and radiosounding (RS) IWV product show good agreement (R^2 0.98).
- Main influence in GNSS-RS differences is due to IWV values (worse as IWV increases).
- SZA and seasonality also influence differences, partly related to IWV values.
- Differences' influence on pressure could be partly related to GNSS' ZHD modeling.
- Clouds do not show a significative influence in GNSS-RS differences.

GRAPHICAL ABSTRACT

ARTICLE INFO

Article history:
Received 25 May 2018
Received in revised form 23 July 2018
Accepted 14 August 2018
Available online 18 August 2018

Editor: Ashantha Goonetilleke

Keywords:
Integrated water vapor
GNSS
Radiosounding
GRUAN
Validation

ABSTRACT

Integrated water vapor (IWV) data from Global Navigation Satellite Systems (GNSS) and radiosounding (RS) are compared over four sites (Lindenberg, Ny-Ålesund, Lauder and Sodankylä), which are part of the Global Climate Observing System (GCOS) Reference Upper Air Network (GRUAN). Both datasets show an excellent agreement, with a high degree of correlation (R^2 over 0.98). Dependences of GNSS-RS differences on several variables are studied in detail. Mean bias error (MBE) and standard deviation (SD) increase with IWV, but in relative term, these variables decrease as IWV increases. The dependence on solar zenith angle (SZA) is partially related to the distribution of IWV with SZA, but the increase of SD for low SZA could be associated with errors in the humidity sensor. Large surface pressures worsen performance, which could be due to the fact that low IWV is typically present in high pressure situations. Cloud cover shows a weak influence on the mentioned MBE and SD. The horizontal displacement of radiosondes generally causes SD to increase and MBE to decrease (increase without sign), as it could be expected. The results point out that GNSS measurements are useful to analyze performance to other instruments measuring IWV.

1. Introduction

Water vapor has a paramount relevance in the climate system, since it is acknowledged as the most important atmospheric greenhouse gas, and despite of not being directly involved in global

* Corresponding author at: Departamento de Física, Universidad de Extremadura, Badajoz, Spain.
E-mail address: javier_vm@unex.es (J. Vaquero-Martínez).

https://doi.org/10.1016/j.scitotenv.2018.08.192
0048-9697/

Table 1
Location of the GNSS stations and days with IWV and ZTD data available.

Site	Corresponding RS site	Latitude (°N)	Longitude (°E)	Altitude (m)	Days with IWV data	Days with ZTD data
ldb0	LIN	52.124	14.070	0.002	2143	2164
ldb2	LIN	52.123	14.072	0.160	138	148
ldrz	LAU	−45.022	169.410	0.380	41	98
nya1	NYA	78.555	11.515	0.084	1873	1898
nya2	NYA	78.555	11.513	0.082	0	27
nyal	NYA	78.555	11.521	0.082	0	0
soda	SOD	67.251	26.232	0.300	36	1402
sodf	SOD	67.216	26.375	0.213	0	1

Table 2
Location of RS stations, distance to GNSS sites, and coincident period for both instruments.

Site	Latitude (°N)	Longitude (°E)	Altitude (m)	Distance (km)	Coincident period
LIN	52.210	14.120	112	10.2	12/11/2012 to 04/15/2015
LAU	−45.050	169.680	370	21.5	06/08/2005 to 01/22/2018
SOD	67.370	26.630	179	21.6	05/21/2006 to 05/02/2017
NYA	78.923	11.923	16	42.1	05/15/2007 to 01/10/2018

warming, it causes a positive radiative feedback on climate system (Colman, 2003, 2015). It also plays a fundamental role in energy transport, evaporating at low latitudes, and being transported to higher latitudes where it condensates, releasing high amounts of latent heat (Myhre et al., 2013).

Integrated water vapor (IWV) is the variable commonly used to study the atmospheric water vapor. IWV is a magnitude equivalent to condensing all the water vapor in the atmospheric vertical column and measuring the height that it would reach if contained in a vessel of unit cross section; being its units those of superficial density (g mm^{-2}) or length (mm).

However, understanding of water vapor effects on climate still needs improving because of the high variability of this gas, both spatially and temporally. It is therefore necessary to retrieve quality water vapor data. Radiosounding (RS) is one of the more precise and direct ways to measure water vapor profiles, and from them IWV

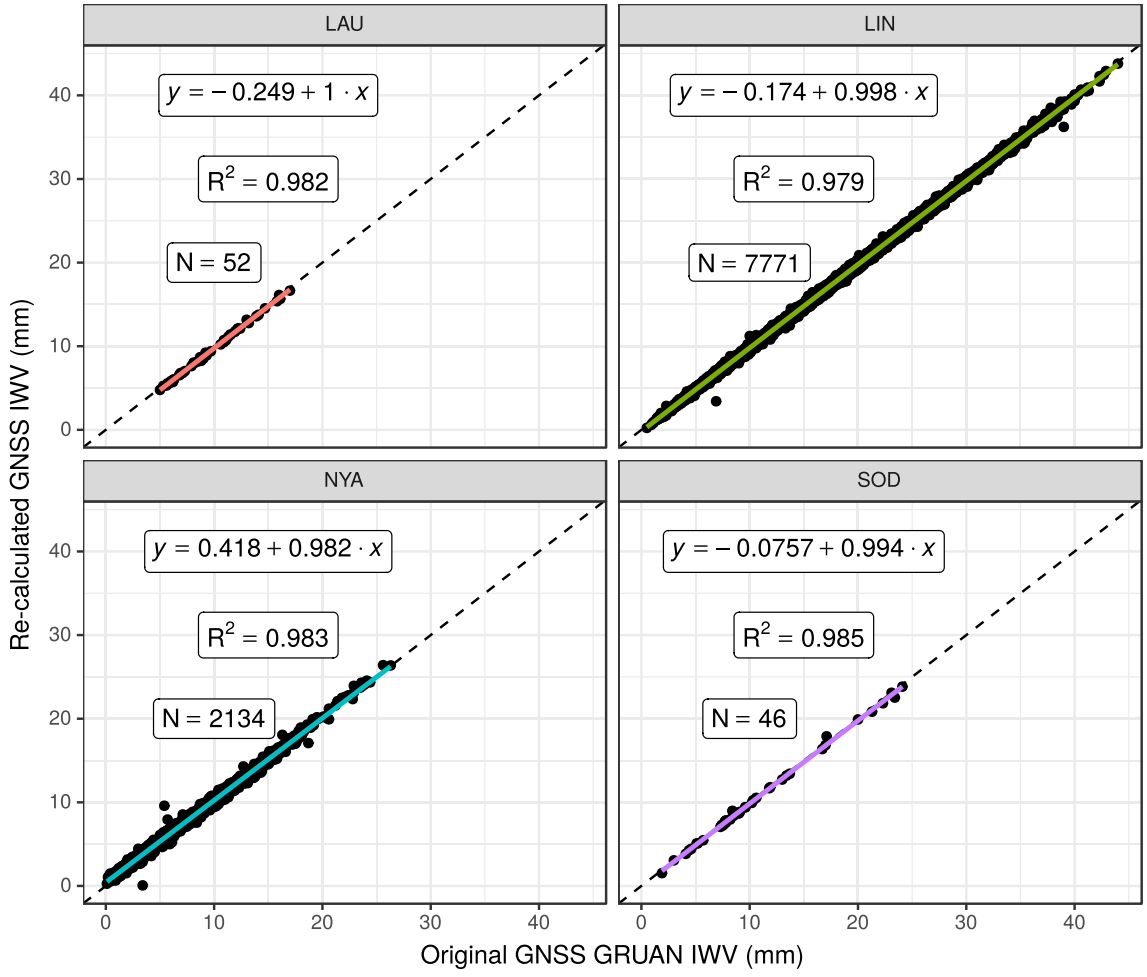

Fig. 1. Scatterplots for GNSS-derived IWV from meteorological data provided by GRUAN (x-axis) and meteorological data provided by radiosounding (y-axis) for the four GRUAN stations. Color, continuous lines are regression lines and black, dashed lines are the identity line.

Table 3
Statistics of the differences GNSS IWV − RS IWV (all in mm, except slope and R^2, which are unitless). MABE is mean absolute bias error, MEDIAN is the median of the differences, IQR is the inter-quartile range of the difference and N the number of data-points.

Site	MBE	SD	MABE	MEDIAN	IQR	N
LAU	−0.767	0.672	0.855	−0.753	0.658	109
LIN	−0.874	1.099	1.094	−0.833	1.150	7837
NYA	−0.492	0.614	0.600	−0.449	0.712	2164
SOD	−0.516	0.830	0.726	−0.435	0.957	2118

data, despite its limitation of temporal resolution (typically one or two launches per day). RS is therefore established as a reference to validate other instruments (du Piesanie et al., 2013; Ohtani and Naito, 2000; Antón et al., 2015). However, it still has some sources of errors as explained in Wang and Zhang (2008) and Dirksen et al. (2014), most of them due to the problem of changes in the radiosonde models and errors in the humidity sensor related to heating by solar radiation.

Moreover, Global Navigation Satellite Systems (GNSS) meteorology is a relatively recent technique that can be used to derive IWV data (Bevis et al., 1992). GNSS measurements have some advantages: all-weather availability, high temporal resolution (5 min to 2 h), high accuracy (less than 3 mm in IWV) and long-term stability. Hence, GNSS data are also used as reference to validate other instruments (Köpken, 2001; Prasad and Singh, 2009; Rama Varma Raja et al., 2008; Román et al., 2015; Vaquero-Martínez et al., 2017a,b, 2018), but as the recent technique that it is, GNSS meteorology still needs validation and assessment of quality in different parts of the Globe.

The Global Climate Observing System (GCOS) Reference Upper-Air Network (GRUAN) has recognized the need of having redundant water vapor measurements in order to improve their quality (GRUAN, 2007). Hence, GRUAN stations that already measure water vapor with RS are being equipped with GNSS receivers and a GRUAN GNSS water vapor product is being developed (WMO, 2008).

The main goal of this study is to analyze the possible errors of the new GNSS IWV products in order to assess their use for other purposes, allowing an improvement in temporal resolution as compared with traditional RS. This way, in this article compare the IWV from GNSS against IWV from RS at the four GRUAN stations with both RS and GNSS water vapor data currently available, and analyze the causes of the differences.

This article is organized as follows: Section 2 describes the different datasets used and their characteristics, and the methodology used in this work. Section 3 includes the results and its discussion, validating the GNSS retrieval performed by the authors for comparison purposes, and analyzing the comparison results. Section 4 summarizes the main conclusions.

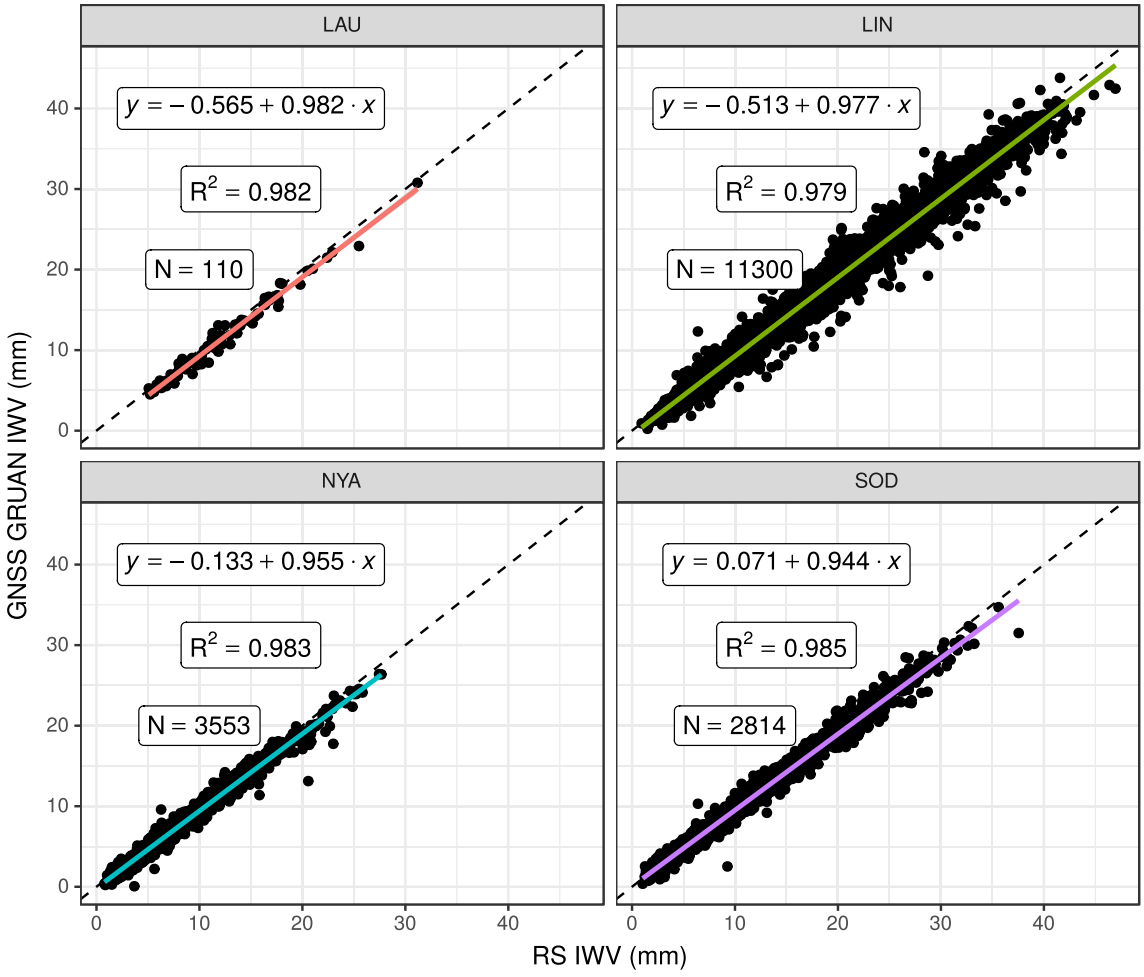

Fig. 2. Scatterplots for GNSS IWV data (y-axis) and RS IWV data (x-axis) for the four GRUAN stations. Color, dashed lines are regression lines and black, continuous lines are the identity line.

2. Material and methods

2.1. IWV from GRUAN GNSS

GNSS consists of a series of satellites that communicate through L-band microwave radiation with receivers, mainly in order to estimate these receivers' locations. The method to obtain IWV from GNSS measurements is detailed in Bevis et al. (1992), and briefly explained in the following lines.

The time spent by the signal in reaching the receiver can be used to calculate the distance between the satellite and receiver, and taking into account the position of the satellites, to obtain the receiver's position. However, several corrections need to be applied, since the signal suffers a series of delays in its travel to the receiver. There is a particular contribution, the Slant Tropospheric Delay (STD), that allows IWV calculation. This contribution refers to the delay that the troposphere causes in the signal, and is referred to the path that the signal follows. Mapping functions (Niell, 2000; Boehm et al., 2006a,b) can be applied to obtain the zenithal equivalent of this amount, the Zenith Tropospheric Delay (ZTD). ZTD is the sum of two contributions, one related to the non-dipolar contribution of all gases in the troposphere (Zenith Hydrostatic Delay, ZHD), and another related to the dipolar contribution of water vapor (Zenith Wet Delay, ZWD) since it is the only compound with dipolar momentum in the atmosphere. A simple model can estimate accurately ZHD (Saastamoinen, 1972), based on surface pressure. This model is accurate to the submilimeter region except if that the hydrostatic equilibrium condition does not hold; in that case errors can reach 1 mm in ZHD. The performance of other models are similar (Opaluwa et al., 2013). Once ZHD is obtained, ZWD can be estimated as ZWD = ZTD − ZHD.

Additionally, another variable is necessary to convert ZWD to IWV, the water vapor weighted mean temperature in the vertical column (T_m). T_m is defined as Eq. (1):

$$T_m = \frac{\int \frac{P_v}{T} dz}{\int \frac{P_v}{T^2} dz}, \quad (1)$$

where P_v is water vapor partial pressure and T is the temperature, both at altitude z. T_m is often estimated from surface temperature from meteorological stations, using empirical fits, or obtained from re-analysis or radiosondes.

The product used in this work is developed by GRUAN GNSS (GG) Precipitable Water Vapour Task Team. Ground-based GNSS IWV has been identified as a Priority 1 measurement for GRUAN. Therefore, a lot of efforts are being done in the last few years to implement this kind of measurements in GRUAN sites. The sites are Lindenberg (LIN), Sodankylä (SOD), Lauder (LAU) and Ny-Ålesund (NYA). Despite the voluntary nature of GG sites, the GG sites must follow a series of guidelines in order to ensure the quality of GG IWV data. Thus, these sites must be equipped with automatic meteorological stations or there must be a nearby station. The GG locations involved in this work are detailed in Table 1.

GRUAN network provides both ZTD and IWV products for those stations equipped with GNSS. However, sometimes meteorological

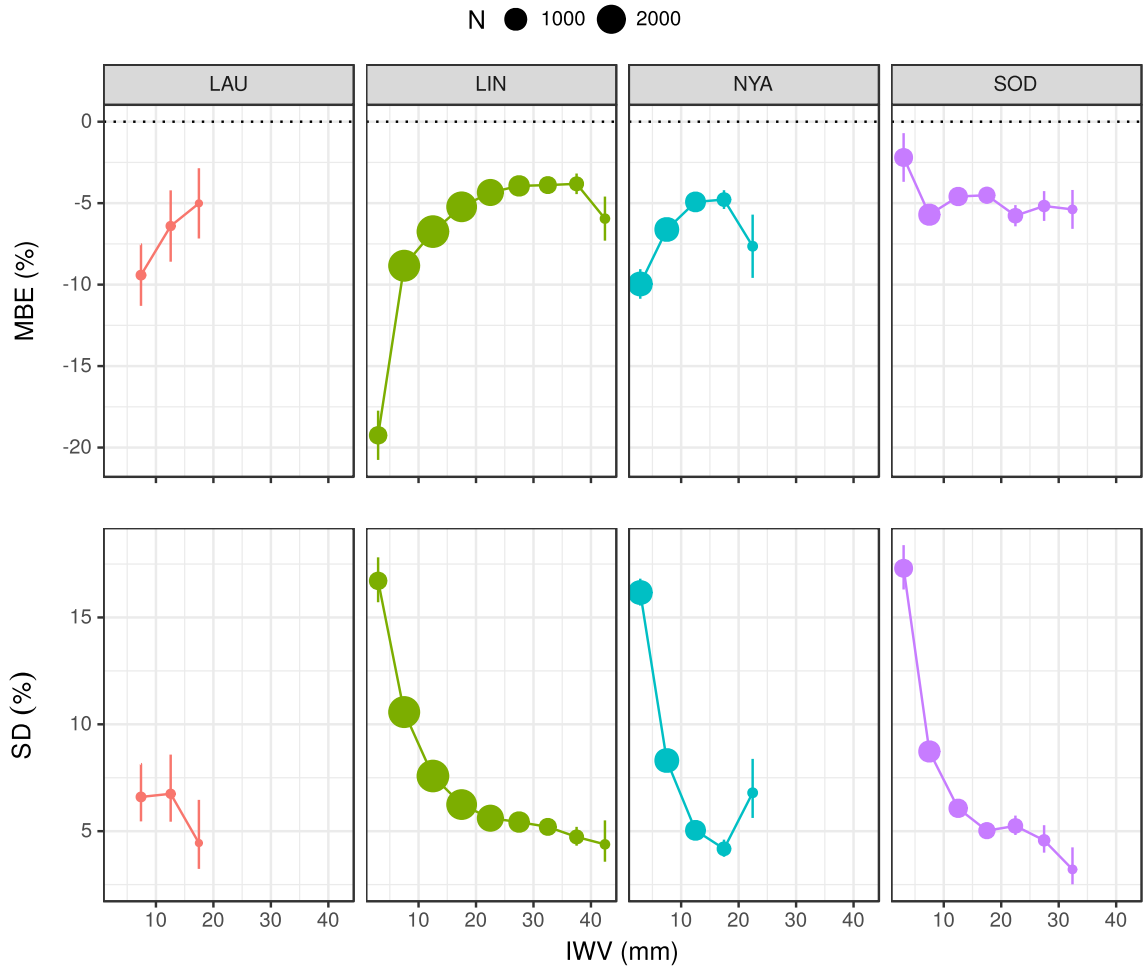

Fig. 3. MBE (top) and SD (bottom) of GNSS-RS differences (%) with respect to IWV from RS for the four GRUAN stations.

data (pressure and temperature) are not available and GRUAN provides only ZTD product. The number of days with GG IWV data at every station available for this study is also shown in Table 1. It can be observed that LAU and SOD stations exhibit a reduced number of days with original GG IWV data. To solve this issue and increase the data number, in this work, GRUAN radiosonde meteorological data (T_m and surface pressure) are used to obtain a new IWV product from GG ZTD data (obtained by authors for comparison purposes only). This new product, developed for comparison purposes, is named in this work as "re-calculated GG IWV product", while the GNSS IWV product retrieved directly from GRUAN have been named as "original GG IWV product". Table 1 shows the number of available days with this re-calculated GG IWV product. It must be noted the notable increase of available days, particularly for LAU and SOD sites. Some restrictions have been applied to ensure data quality:

- Resulting values of IWV must make sense (0 mm < IWV < 100 mm).
- Mean weighted temperature must be lower than 500 K and positive.

2.2. Radiosoundings from GRUAN network

GRUAN network provides radiosonde data for 28 sites. We have considered those sites that also have a nearby GNSS product from GRUAN. Table 2 shows the locations of the four sites considered in this work.

Typically the radiosonde launches are at specific hours. LIN typically has 4 launches a day (00, 06, 12, 18 h), while NYA's sondes are typically launched at 12 h, and some launches at other hours, specially at 00, 06, and 18 h. Sondes at SOD are launched at 00 and 12 h (some others at different hours), and at LAU at different hours (approximately one launch per week).

The radiosondes that provide the data in this work are Vaisala RS92. The RS92 model is equipped with a wire-like capacitive temperature sensor ("thermocap"); two polymer capacitive moisture sensor ("humicap"), a silicon-based pressure sensor and a GPS receiver. More detailed information about the processing of the data retrieved can be found at https://www.gruan.org/instruments/radiosondes/sonde-models/vaisala-rs92/ or Dirksen et al. (2014). The main error sources that affect the humidity sensor are daytime solar heating of the Humicaps (introduces a dry bias), sensor time-lag at temperatures below about −40° (this is not a problem in this work) and temperature dependent calibration correction.

The GRUAN RS92 product includes data on profiles of pressure, temperature, humidity, relative humidity, water vapor mixing ratio, wind information, frostpoint, short-wave radiation, and associated uncertainties. IWV can be calculated by integration of water vapor mixing ratio (WVMR) in pressures as Eq. (2):

$$\mathrm{IWV} = \int_0^{p_s} \mathrm{WVMR} \cdot \mathrm{d}p, \tag{2}$$

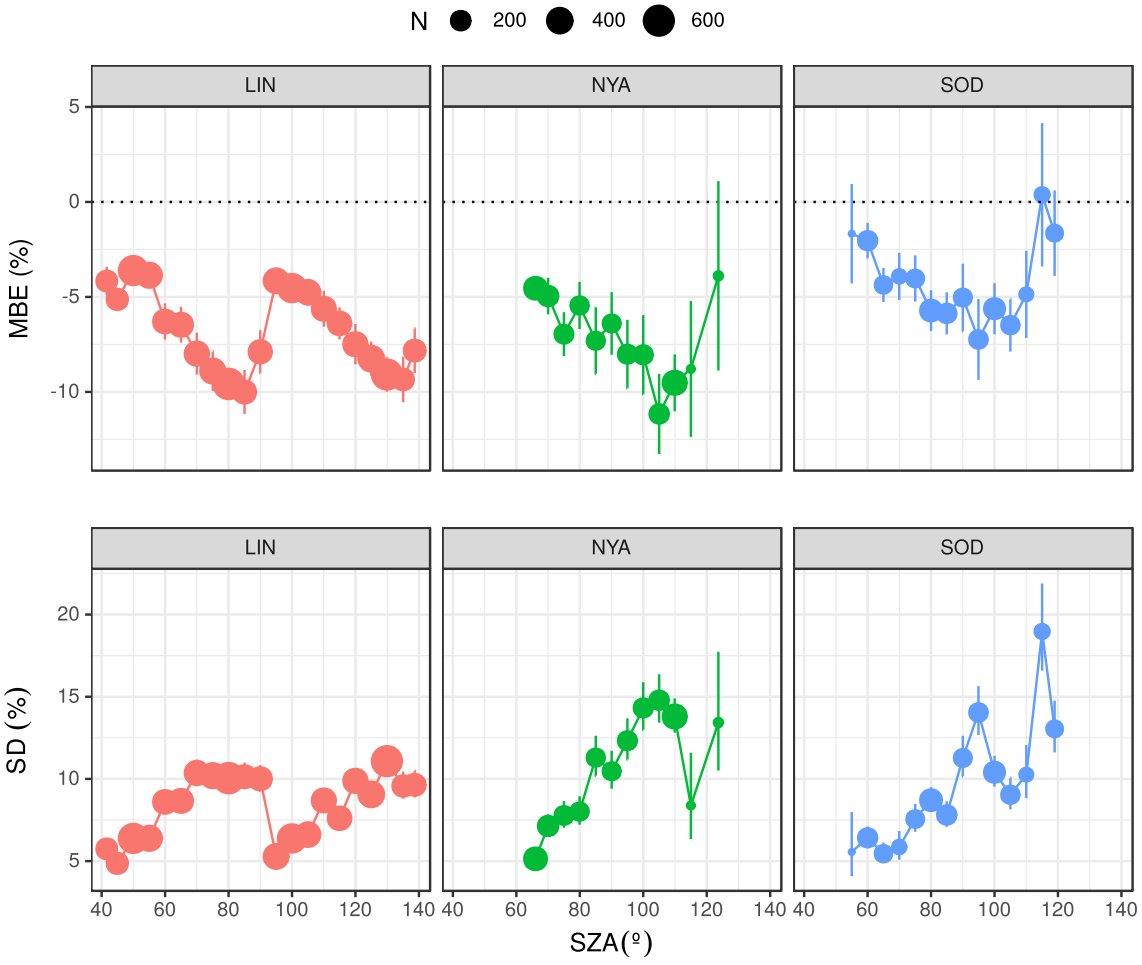

Fig. 4. MBE (top) and SD (bottom) of GNSS-RS differences (%) with respect to SZA for three GRUAN stations.

where WVMR is the water vapor mixing ratio, p is the pressure and p_s the surface pressure. In addition, some restrictions have been considered in order to ensure GRUAN data quality:

- Number of levels must be more than 15.
- First level must be at height lower than 1 km.
- Last level must be at height larger than 9 km.
- Resulting values of IWV must make sense $0\,\text{mm} < \text{IWV} < 100\,\text{mm}$.

2.3. Methodology

The followed criterion to match the GNSS and RS data require that time differences between RS launch and GNSS measurement must be below 30 min. For the analysis of differences, RS measurements have been considered as reference and two variables have been analyzed, physical difference (GNSS minus RS) and relative difference (difference divided by RS value). The mean of the differences (also known as mean bias error, MBE) and the standard deviation of the differences (SD) have been calculated. The SD have been used as a measurement of precision and the MBE as measurement of accuracy. The MBE is calculated as Eq. (3):

$$\text{MBE} = \frac{1}{N}\sum_{i}^{N}\delta_i, \tag{3}$$

where δ_i are the physical differences (absolute MBE) or the relative differences (relative MBE). Moreover the SD is obtained as Eq. (4):

$$\text{SD} = \sqrt{\frac{1}{N-1}\sum_{i}^{N}\left(\delta_i - \bar{\delta}_i\right)}. \tag{4}$$

In order to study whether these differences depend on other variables or not, the data have been divided into several bins of similar values of these variables for the study of the precision and accuracy of IWV in each bin. It must be noticed that data bins with less than 15 data have been rejected, as not representative.

3. Results and discussion

3.1. Original GG IWV data vs re-calculated GG IWV data

Fig. 1 shows the correlation between the original and re-calculated GG IWV data. In all stations both data-sets exhibit an excellent agreement ($R^2 \sim 0.99$). All stations show negative offsets (except NYA, which is positive), but all are quite small, less than 0.4 mm in all cases. Outliers, like the ones in NYA and LIN (differences of more than 1.5 mm in IWV), are mainly caused by the differences in pressure measurements. However, around 90% of the data pairs differ by less than 0.7 mm.

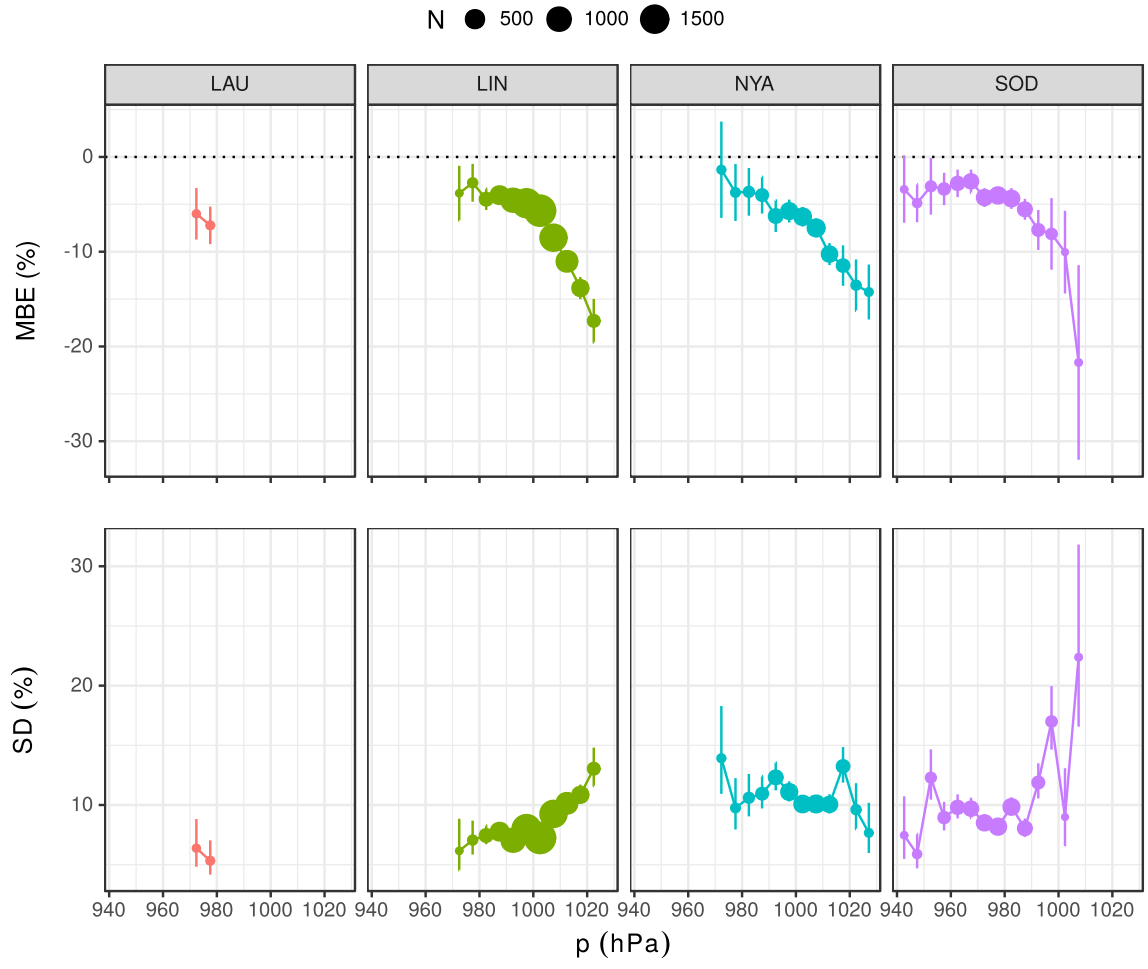

Fig. 5. MBE (top) and SD (bottom) of GNSS-RS differences (%) with respect to pressure for the four GRUAN stations.

Therefore, the data-set of GNSS-derived IWV using meteorological data from radiosonde (GNSSRS) represents very well GRUAN's IWV product. In order to have a data-set with the same features, all the data used in this work will come from the GNSS-derived IWV using meteorological data from radiosonde. The advantages of using this data-set are as follows:

1. More data is available (particularly at SOD and LAU stations).
2. Davis "mean" temperature can be obtained directly from radiosonde.
3. Temporal interpolation is not necessary.

Needless to say, this is only for comparison purposes, since the radiosonde meteorological data is typically available for at most four times a day, and the GNSS products are available every 15 min.

3.2. Comparison between GNSS IWV and RS IWV

3.2.1. Overall statistics and regressions

Table 3 shows a summary of the statistics of the differences between IWV from GNSS and RS. MBE values are over −0.9 mm for all stations, being closer to zero for NYA and SOD (around 0.5 mm). SD values are around 0.6–1 mm. Median and MBE values are similar, which indicates that the differences distributions are most likely normal. Fig. 2 shows the regression lines. Both data-sets are in agreement with R^2 around 0.98.

The differences GNSS-RS and relative differences are analyzed in this section in order to find dependence on different variables. The differences are distributed into bins of similar values of the variable analyzed, and the evolution of MBE and SD over the different bins is analyzed. It must be noticed that the data bins with less than 15 data are not shown, as they are not considered representative.

3.2.2. Dependence of GNSS-RS differences on IWV

The available data-set have been divided into bins of 5 mm. All stations have a very similar behaviour with respect to IWV. The relative MBE in Fig. 3 (top) shows that there is a dry bias (around 5%) that decreases in absolute value with IWV. However, for SOD first bin is closer to zero (~2.5%) than the rest of the bins (~5%) of SOD. Absolute MBE (not shown) typically increases in absolute value with IWV, ranging from less than −1 mm up to −2 or −2.5 mm. Such small range explains the behaviour of relative MBE: absolute differences do not change much, but the reference IWV does, thus the relative value decrease (in absolute value) as IWV increases.

Regarding precision (see Fig. 3, bottom), relative SD, decrease as IWV increases, reaching a minimum of around 5% in all cases for IWV above 15 mm. Despite the different ranges of IWV and number of data of each station, the relative SD is very similar in the lowest bin, between 15 and 17%). A similar interpretation to that of the MBE is appropriate here: SD in absolute terms increases with IWV, but in a range (0.5–2 mm) that is quite smaller than the range of IWV itself (0–40 mm), and therefore relative SD tends to decrease with increasing IWV. Unfortunately, LAU available data does not show a wide range of IWV, so it is difficult to interpret the results, but they are compatible with those observed in the rest of sites, with values around 5–7% in the range of 5–20 mm. A similar behaviour was observed in other comparisons between GNSS and satellite products (Román et al., 2015; Vaquero-Martínez et al., 2017a,b, 2018) and

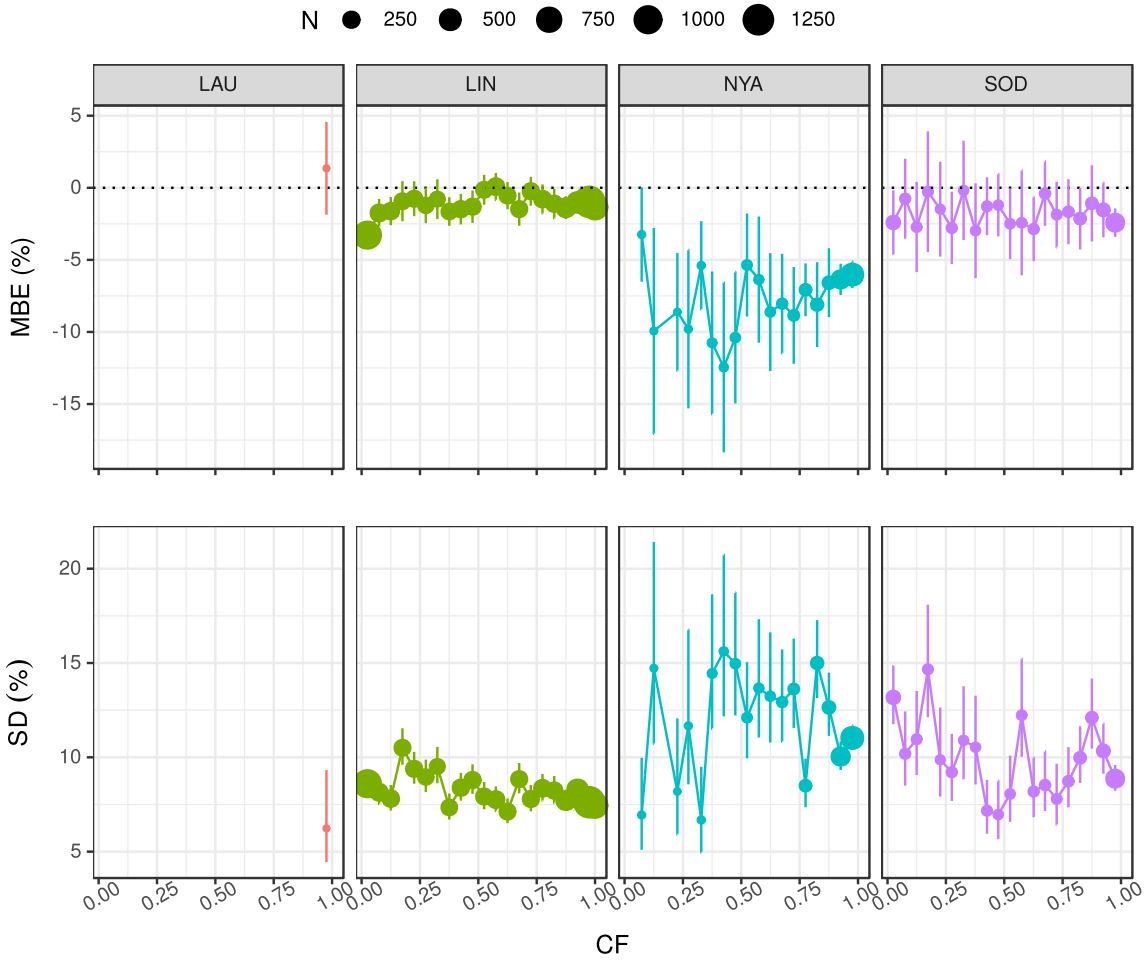

Fig. 6. MBE (top) and SD (bottom) of GNSS-RS differences (%) with respect to cloud fraction (CF) for the four GRUAN stations.

between RS and satellite products (Antón et al., 2015). Correlation coefficient R decreases as IWV increases (not shown), from values over 0.8 for low IWV to values below 0.7 for IWV above 30 mm.

3.2.3. Dependence of GNSS-RS differences on SZA

Differences related to SZA could be due to errors in radiosonde sensors (especially humidity sensor, which is affected by solar radiation), as stated in Wang and Zhang (2008) and Dirksen et al. (2014). Fig. 4 (top) shows relative MBE of every 5° bins. It must be noticed that LAU does not have bins with enough (>15) data, so its results are not considered.

Although there are some differences between stations, relative MBE generally worsens as SZA increases. LIN shows a sharp increase at SZA = 90° (sunrise and sunset), while worsening of MBE with SZA is more monotonous at SOD and NYA, with some increase from 110°. These behaviours are quite related to typical values of IWV for those SZA bins, especially at LIN: low SZA causes higher temperatures, which causes the atmosphere to accept more water vapor and therefore causes IWV to increase. The distribution of IWV with SZA was checked, confirming this hypothesis. Also, an interesting feature at LIN IWV was found: SZA increases rapidly around 90° and decreases for SZA above that value. As NYA and SOD are Arctic stations, the influence of SZA is not so marked. Values are typically between 5 and 10%. GOME-2 water vapor product exhibits a similar behaviour, as shown in Antón et al. (2015), but the sign of MBE is positive in that case. Differences between day and night are not important, although in Wang and Zhang (2008) Vaisala RS92 showed a worse performance at day than at night.

In relative terms, as Fig. 4 (bottom) reveals, SD increases with SZA. At nighttime, relative SD is higher and more stable, and at daytime, it is lower and has a increasing tendency with SZA. Minimum relative SD for all stations is around 5%, but the maximum differs (10% for LIN, 15% for NYA, and 20% for SOD). This behaviour can be partially due to the observed increase in relative SD for low IWV, with a similar argument to the one provided for relative MBE in this section. In absolute terms (not shown), SD decreases with SZA, which is consistent with this argument, but it could also be related to the fact that at low SZA the radiosondes humidity sensor can be affected by solar radiation (Dirksen et al., 2014; Wang and Zhang, 2008) and partly because of the typically higher IWV values at low SZA. Several satellite product showed similar behaviour (but with less precision) (Vaquero-Martínez et al., 2018).

In this subsection, it is also analyzed the seasonal dependence of GNSS-RS differences. SZA and IWV both have annual cycles, which cause the MBE and SD of the differences between IWV from GNSS and RS to have a seasonal dependence as well. LIN and NYA exhibit (not shown) slightly worse relative MBE in winter (low IWV) than in summer, while SOD (not shown) has worse relative MBE at summer (higher IWV). Relative SD in LIN, NYA and SOD are smaller at summer (low SZA) than in winter. The hypothesis that seasonal dependence on water vapor products performance is mainly affected by dependences on IWV and SZA is also proposed in other works

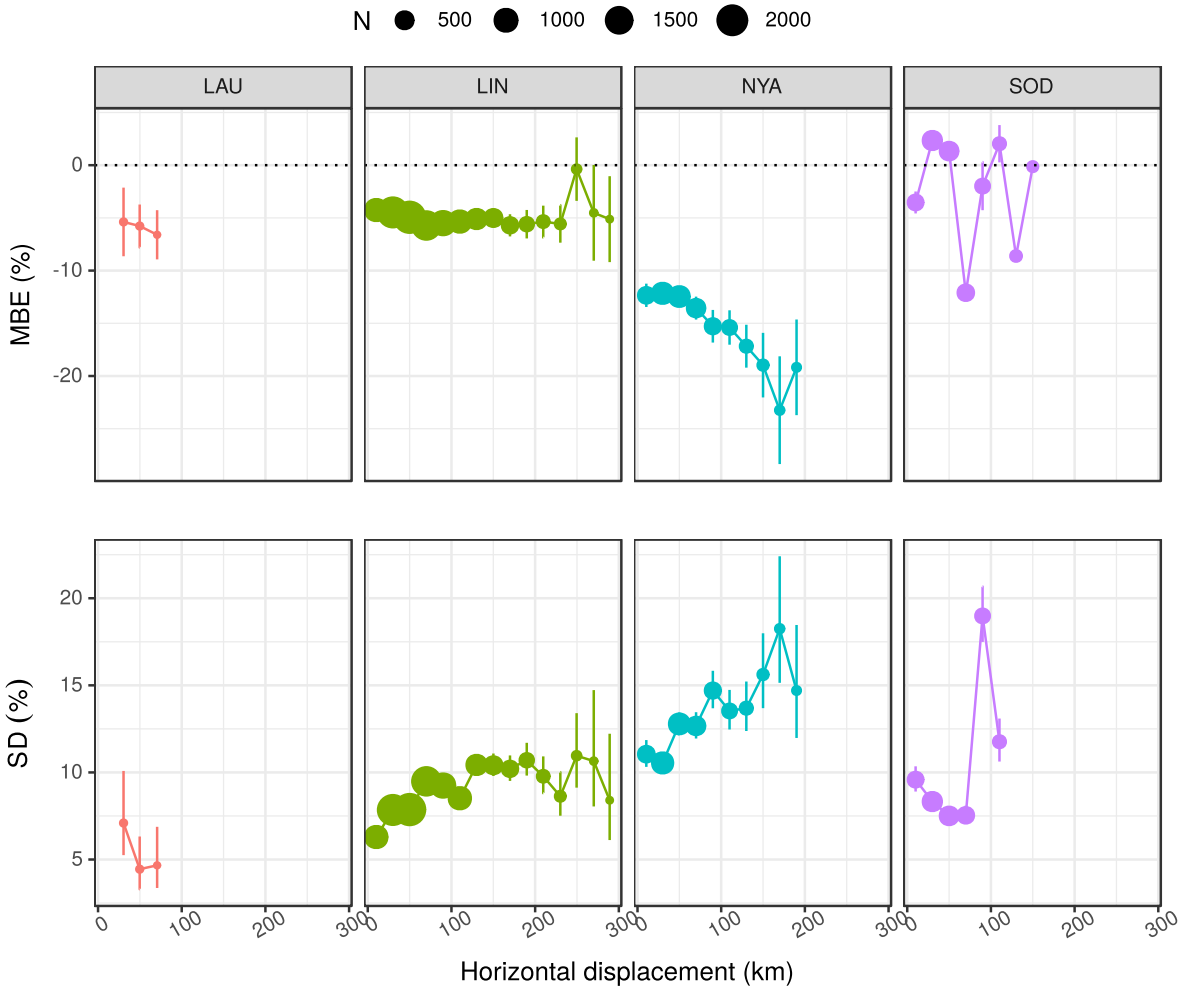

Fig. 7. MBE (top) and SD (bottom) of GNSS-RS differences (%) with respect to RS displacement for the four GRUAN stations.

where satellite products are compared with GNSS ground-based measurements (Vaquero-Martínez et al., 2017a,b, 2018).

3.2.4. Dependence on pressure

Surface pressure also affects to the GNSS-RS differences. Fig. 5 (top) shows the MBE each 5 hPa bins. Relative MBE increases without sign as pressure increases. Values are between −15% and 0% approximately. At high pressures, MBE worsens at a sharper rate. This could be caused by the distribution of IWV with surface pressure: at high pressure, IWV is smaller, being the relative MBE higher. Another explanation that could contribute partially to this behaviour is related to the way that GNSS IWV is retrieved, since the surface pressure is needed in Saastamoinen's model (Saastamoinen, 1972).

Relative SD, shown in Fig. 5) (top), increases with pressure. Values are between 5–10% (LIN), around 10% (NYA) and 5–20% (SOD). LAU shows slight lower values, around 5% but these values are only for low IWV pressure values. As it also happens with MBE, this behaviour could be partially due to the distribution of IWV with pressure: lower values of IWV are generally registered at higher values of pressure. SD in absolute terms (not shown) exhibits a maximum (1000 hPa for LIN, 980 hPa for SOD) that is coincident with a maximum in typical IWV values.

3.2.5. Dependence of GNSS-RS differences on cloudiness

Total cloud cover data have been obtained from Era-Interim Reanalysis (Dee et al., 2011), and co-located to the sites and times of IWV measurements. These data are in the form of cloud fraction (CF), that is to say, a number between 0 (no clouds) and 1 (totally covered) indicating the pixel cloud cover.

Relative MBE, as shown in Fig. 6 (top), is above −4% for LIN and SOD, and between −4 and 12% for NYA. LAU only counts with 1 point, positive relative MBE (less than 2%). However, the results do not show any dependence of MBE on CF. MBE in absolute terms does not show any dependence on CF either.

Regarding relative SD, no tendency is observed (see Fig. 6 (bottom)). LIN has very stable values around 8%. NYA however, have highly variable values of SD, some around 7%, other more than 12%, with high uncertainties. Nevertheless, SOD exhibits a slight tendency to decrease SD as CF increases, although still with high variability (between 7% and 15%) and uncertainties.

3.2.6. Dependence on radiosonde horizontal movement

Radiosondes usually move horizontally due to winds. This could be a source of error (Seidel et al., 2011), so it must be taken into account. The distance is obtained as the horizontal distance between the first (closest to the ground) and last (furthest from the ground) radiosonde positions. 20 km bins have been used to study the evolution of MBE and SD throughout the distances.

Fig. 7 (top) clearly shows that relative MBE is farther from zero as horizontal displacement increases at NYA, but there is no important trend for the other sites. A reason for this could be that NYA site is located in the Island of Spitsbergen, meaning that a displacement can put the radiosonde over the sea, where differences with the genuine water vapor vertical profile can be more important. SOD shows a very high variability, which could be due to inhomogeneous terrain (and thus, humidity) in the vicinity of the site. Relative MBE changes from −4% to −9% at LIN, and from −10% to −20% at NYA.

Fig. 7 (bottom) shows the relative SD for several horizontal bins, which clearly increases as the horizontal displacement increases, which is to be expected. LIN goes from 5% to 15%, NYA from 10% to 20%, and SOD from 0% to 20%. It must be noted the high variability in SOD relative SD values, which can be caused by the inhomogeneity of the humidity fields in the vicinity around the site.

4. Conclusions

Global Climate Observing System (GCOS) Reference Upper Air Network (GRUAN)'s Global Navigation Satellite System (GNSS) and radiosonde (RS) integrated water vapor (IWV) products are in agreement at the sites considered. The regression analysis showed a high correlation ($R^2 > 0.98$) and certain offset that can be due to the spatial separation between GNSS and RS stations. The intercept is positive for all stations except NYA, and the magnitude ranges around 0.1–0.2 mm. Values of the standard deviation of the differences (SD) are between 0.6 and 1 mm.

The study on dependences of the GNSS-RS differences showed that the mean of the differences (MBE) and SD generally increase (omitting the sign of MBE) with IWV, although relative MBE and SD showed the opposed behaviour. Performance of RS IWV product was expected to worsen at low solar zenith angle (SZA) because of errors in humidity sensor of radiosondes but this was not observed, so corrections are being applied correctly. However, SD does increase at low SZA. Most of the observed dependences on SZA are probably related to the distribution of IWV with SZA (IWV is larger at low SZA, when the temperatures are higher). The dependences on SZA and IWV also cause a seasonal dependence.

MBE (without sign) and SD exhibits an increase with increasing surface pressure, that can be partially due to the distribution of IWV with pressure (IWV is smaller at high pressures), and partially to errors in the modeling of ZHD through Saastamoinen's model. However, this is an issue that shall be studied closely in future work. Cloud cover did not show a significant influence on MBE and SD. Regarding dependence on horizontal displacement of radiosondes, the relative MBE and SD show that the performance of RS is poorer when the horizontal displacement is larger, although this seems to be very influence by the characteristics of the site's vicinity.

In summary, the GNSS and RS values are very similar and the dependences on other factors low, but it should be pointed out that it is still very necessary to have redundant measurements of water vapor in order to improve both the quality of measurements and the sampling of the data. GNSS exhibits two important advantages: first the high temporal resolution, and second the stability against the sky conditions (wind, clouds, etc.), which make GNSS IWV measurement particularly well suited for comparison purposes. However, it must be noticed that the low number of stations do not allow to extract conclusions over the whole range of the variables studied, mainly IWV and SZA.

Acknowledgments

Support from the Junta de Extremadura (Research Group Grant GR15137) is gratefully acknowledged. Work at the Universidad de Valladolid is supported by project CMT2015-66742-R. The authors wish to thank the operators at the four observatories (Lindenberg, Lauder, Ny-Ålesund and Sodankylä) for dutifully performing reference radiosoundings and maintenance of GNSS according to the GRUAN standards, as well as GFZ Helmholtz Center Postdam for their processing of GNSS data products to obtain ZTD and IWV, and acknowledge ERA-Interim data.

References

Antón, M., Loyola, D., Román, R., Vömel, H., 2015. Validation of GOME-2/MetOp-a total water vapour column using reference radiosonde data from the GRUAN network. Atmos. Meas. Tech. 8, 1135–1145. https://doi.org/10.5194/amt-8-1135-2015.

Bevis, M., Businger, S., Herring, T.A., Rocken, C., Anthes, R.A., Ware, R.H., 1992. GPS meteorology: remote sensing of atmospheric water vapor using the global positioning system. J. Geophys. Res. 97, 15787–15801. https://doi.org/10.1029/92JD01517. URL: http://doi.wiley.com/10.1029/92JD01517.

Boehm, J., Niell, A., Tregoning, P., Schuh, H., 2006a. Global mapping function (GMF): a new empirical mapping function based on numerical weather model data. Geophys. Res. Lett. 33, 3–6. https://doi.org/10.1029/2005GL025546.

Boehm, J., Werl, B., Schuh, H., 2006b. Troposphere mapping functions for GPS and very long baseline interferometry from European Centre for Medium-Range Weather Forecasts operational analysis data. J. Geophys. Res. Solid Earth 111, 1–9. https://doi.org/10.1029/2005JB003629.

Colman, R., 2003. A comparison of climate feedbacks in general circulation models. Clim. Dyn. 20, 865–873. http://arXiv:183550600013. https://doi.org/10.1007/s00382-003-0310-z. URL: http://link.springer.com/article/10.1007/s00382-003-0310-z.

Colman, R.A., 2015. Climate radiative feedbacks and adjustments at the Earth's surface. J. Geophys. Res. Atmos. 120, 3173–3182. https://doi.org/10.1002/2014JD022896. URL: http://doi.wiley.com/10.1002/2014JD022896.

Dee, D.P., Uppala, S.M., Simmons, A.J., Berrisford, P., Poli, P., Kobayashi, S., Andrae, U., Balmaseda, M.A., Balsamo, G., Bauer, P., Bechtold, P., Beljaars, A.C.M., van de Berg, L., Bidlot, J., Bormann, N., Delsol, C., Dragani, R., Fuentes, M., Geer, A.J., Haimberger, L., Healy, S.B., Hersbach, H., Hólm, E.V., Isaksen, L., Kållberg, P., Köhler, M., Matricardi, M., McNally, A.P., Monge-Sanz, B.M., Morcrette, J.-J., Park, B.-K., Peubey, C., de Rosnay, P., Tavolato, C., Thépaut, J.-N., Vitart, F., 2011. The ERA-Interim reanalysis: configuration and performance of the data assimilation system. Q. J. R. Meteorol. Soc. 137, 553–597. https://doi.org/10.1002/qj.828.

Dirksen, R.J., Sommer, M., Immler, F.J., Hurst, D.F., Kivi, R., Vömel, H., 2014. Reference quality upper-air measurements: GRUAN data processing for the Vaisala RS92 radiosonde. Atmos. Meas. Tech. 7, 4463–4490. https://doi.org/10.5194/amt-7-4463-2014. URL: http://www.atmos-meas-tech.net/7/4463/2014/.

du Piesanie, A., Piters, A.J.M., Aben, I., Schrijver, H., Wang, P., Noël, S., 2013. Validation of two independent retrievals of SCIAMACHY water vapour columns using radiosonde data. Atmos. Meas. Tech. 6, 2925–2940. https://doi.org/10.5194/amt-6-2925-2013. URL: http://www.atmos-meas-tech.net/6/2925/2013/.

GRUAN, 2007. Justification, Requirements, Siting, and Instrumentation Options.URL: https://www.gruan.org/gruan/editor/documents/gcos/gcos-112.pdf.

Köpken, C., 2001. Validation of integrated water vapor from numerical models using ground-based GPS, SSM/I, and water vapor radiometer measurements. J. Appl. Meteorol. 40, 1105–1117. ISSN 0894-8763. https://doi.org/10.1175/1520-0450(2001)040<1105:VOIWVF>2.0.CO;2. URL: http://journals.ametsoc.org/doi/abs/10.1175/1520-0450%282001%29040%3C1105%3AVOIWVF%3E2.0.CO%3B2.

Myhre, G., Shindell, D., Bréon, F.-M., Collins, W., Fuglestvedt, J., Huang, J., Koch, D., Lamarque, J.-F., Lee, D., Mendoza, B., Nakajima, T., Robock, A., Stephens, G., Takemura, T., Zhang, H., 2013. Anthropogenic and natural radiative forcing. Climate Change 2013: The Physical Science Basis. Contribution of Working Group I to the Fifth Assessment Report of the Intergovernmental Panel on Climate Change. IPCC., pp. 659–740. (Ipcc ed.).

Niell, A.E., 2000. Improved atmospheric mapping functions for VLBI and GPS. Earth Planets Space 52, 699–702. https://doi.org/10.1186/BF03352267. URL: http://earth-planets-space.springeropen.com/articles/10.1186/BF03352267.

Ohtani, R., Naito, I., 2000. Comparisons of GPS-derived precipitable water vapors with radiosonde observations in Japan. J. Geophys. Res. Atmos. 105, 26917–26929. https://doi.org/10.1029/2000JD900362. URL: http://doi.wiley.com/10.1029/2000JD900362.

Opaluwa, Y.D., Adejare, Z.A.T., Abazu, I.C., Adewale, T.O., Odesanmi, A.O., Okorocha, V.C., 2013. Comparative analysis of five standard dry tropospheric delay models for estimation of dry tropospheric delay in GNSS positioning. Am. J. Geogr. Inf. Syst. 11.

Prasad, A.K., Singh, R.P., 2009. Validation of MODIS Terra, AIRS, NCEP/DOE AMIP-II Reanalysis-2, and AERONET Sun photometer derived integrated precipitable water vapor using ground-based GPS receivers over India. J. Geophys. Res. 114, D05107. http://arXiv:16510847. https://doi.org/10.1029/2008JD011230. URL: http://doi.wiley.com/10.1029/2008JD011230.

Rama Varma Raja, M.K., Gutman, S.I., Yoe, J.G., McMillin, L.M., Zhao, J., 2008. The validation of AIRS retrievals of integrated precipitable water vapor using measurements from a network of ground-based GPS receivers over the contiguous United States. J. Atmos. Ocean. Technol. 25, 416–428. https://doi.org/10.1175/2007JTECHA889.1.

Román, R., Antón, M., Cachorro, V., Loyola, D., Ortiz de Galisteo, J., de Frutos, A., Romero-Campos, P., 2015. Comparison of total water vapor column from GOME-2 on MetOp-A against ground-based GPS measurements at the Iberian Peninsula. Sci. Total Environ. 533, 317–328. http://arXiv:26172599. https://doi.org/10.1016/j.scitotenv.2015.06.124. URL: http://linkinghub.elsevier.com/retrieve/pii/S0048969715303260.

Saastamoinen, J., 1972. Atmospheric correction for the troposphere and stratosphere in radio ranging satellites. In: Henriksen, S.W., Mancini, A., Chovitz, B.H. (Eds.), Geophysical Monograph Series. American Geophysical Union., pp. 247–251. URL: http://doi.wiley.com/10.1029/GM015p0247. https://doi.org/10.1029/GM015p0247.

Seidel, D.J., Sun, B., Pettey, M., Reale, A., 2011. Global radiosonde balloon drift statistics. J. Geophys. Res. 116, https://doi.org/10.1029/2010JD014891. URL: http://doi.wiley.com/10.1029/2010JD014891.

Vaquero-Martínez, J., Antón, M., Ortiz de Galisteo, J.P., Cachorro, V.E., Álvarez-Zapatero, P., Román, R., Loyola, D., Costa, M.J., Wang, H., Abad, G.G., Noël, S., 2018. Inter-comparison of integrated water vapor from satellite instruments using reference GPS data at the Iberian Peninsula. Remote Sens. Environ. 204, 729–740. https://doi.org/10.1016/j.rse.2017.09.028. URL: http://linkinghub.elsevier.com/retrieve/pii/S0034425717304406.

Vaquero-Martínez, J., Antón, M., Ortiz de Galisteo, J.P., Cachorro, V.E., Costa, M.J., Román, R., Bennouna, Y.S., 2017a. Validation of MODIS integrated water vapor product against reference GPS data at the Iberian Peninsula. Int. J. Appl. Earth Obs. Geoinf. 63, 214–221. http://arXiv:27988187. https://doi.org/10.1016/j.jag.2017.07.008. URL: http://linkinghub.elsevier.com/retrieve/pii/S0048969716327176.

Vaquero-Martínez, J., Antón, M., Ortiz de Galisteo, J.P., Cachorro, V.E., Wang, H., González Abad, G., Román, R., Costa, M.J., 2017b. Validation of integrated water vapor from OMI satellite instrument against reference GPS data at the Iberian Peninsula. Sci. Total Environ. 580, 857–864. https://doi.org/10.1016/j.scitotenv.2016.12.032. URL: http://linkinghub.elsevier.com/retrieve/pii/S0048969716327176.

Wang, J., Zhang, L., 2008. Systematic errors in global radiosonde precipitable water data from comparisons with ground-based GPS measurements. J. Clim. 21, 2218–2238. https://doi.org/10.1175/2007JCLI1944.1.

WMO, 2008. Report of the GCOS Reference Upper-air Network Implementation Meeting. https://www.gruan.org/gruan/editor/documents/gcos/gcos-121.pdf.